SYNTHESIS AND EVALUATION OF TOXICITY AND ANTIMICROBIAL ACTIVITY OF RIFAMPICIN ASSOCIATED WITH IRON OXIDE NANOPARTICLES

Joyce Farias Louza DE SOUSA[1] (iD), Plínio Lázaro Faleiro NAVES[1] (iD), Luciana Rebelo GUILHERME[1] (iD)

[1] Postgraduate Program in Sciences Applied to Health Products, Universidade Estadual de Goiás, Anápolis, Goiás, Brazil.

Corresponding author:
Luciana Rebelo Guilherme
luciana.guilherme@ueg.br

Abstract

Rifampicin has broad-spectrum antimicrobial activity, but it can cause nephrotoxic and hepatotoxic damage because high doses are required. Nanosystems emerge as a perspective to improve the transport systems of this drug. In this work, iron oxide nanoparticles were synthesised, functionalized with lauric acid, and rifampicin was incorporated into the nanosystem. The samples were characterized by spectroscopic techniques: electronics in the visible ultraviolet region (UV-vis), vibrational absorption in the infrared region (IR), X-ray diffractometry (XRD), and dynamic light scattering (DSL). The toxicity of the nanocompounds and the antimicrobial activity against *Staphylococcus aureus* ATCC 25923 were studied by the *Artemia salina* lethality and disc diffusion techniques, respectively. As a result, IR analysis showed characteristic vibrations of laurate and rifampicin on the surface of the nanosystem. The presence of magnetic iron oxide was confirmed by XRD and the mean diameter of the crystallites was 8.37 nm. The hydrodynamic diameter of rifampicin associated with the nanosystem was 402 nm and that of the nanosystem without rifampicin was 57 nm. The compounds did not show toxicity to *Artemia salina* and the *in vitro* antimicrobial activity against *Staphylococcus aureus* was slightly decreased when rifampicin was associated with the nanosystem. In general terms, the results showed that iron oxide nanoparticles showed no toxicity and reduced the toxicity of rifampicin by 41.54% when carried compared to free rifampicin. Therefore, magnetic iron oxide nanoparticles may have the potential to act as a platform for associated drugs.

Keywords: Antimicrobial. *Artemia salina.* Brine shrimp. Magnetic nanoparticles. Nanotoxicity. *Staphylococcus aureus*.

1. Introduction

Rifampicin (RIF) is used in the treatment of leprosy, against *Staphylococcus aureus* infections, prophylaxis of meningococcal infection, and influenza (Perumal et al. 2020). It is also widely used in the treatment of tuberculosis against *Mycobacterium tuberculosis* (Adams et al. 2021). However, administration of high doses is necessary to exert its bactericidal activity, this can cause an increase in serum levels of bilirubin and hepatic enzymes, possibly causing hepatotoxicity and, less frequently, the development of acute interstitial nephritis and glomerulonephritis (Legout et al. 2014; Motta et al. 2020). In addition, mutations in RNA polymerase subunits confer antimicrobial resistance to RIF (Goldstein 2014).

To decrease the incidence of problems like those reported above, Ruckh et al. (2012) used nanostructures obtained by poly(caprolactone) electrowinning for RIF transport. The result against

Pseudomonas aeruginosa and *Staphylococcus epidermidis* was minimal colonisation of the structures by both organisms compared to free RIF. Woźniak-Budych et al. (2017) presented the antimicrobial properties of copper and RIF-loaded copper nanoparticles against *Staphylococcus aureus*, *Escherichia coli, Bacillus pumilus,* and *Pseudomonas fluorescens*. The results of the work indicate that the adsorption of rifampicin on the surface of copper nanoparticles can provide the reduction of the antibiotic dosage and prevent its adverse side effects.

It is assumed that magnetic nanoparticles, when associated with other drugs, can direct the drug to its site of action due to their magnetic properties (Khan et al. 2022). By being functionalized to polymers or surfactants, nanoparticles can reduce side effects and toxicity by reducing interactions with other organs or tissues (Yen et al. 2013). Functionalization agents can modulate drug release in the body (Laurent et al. 2008). This characteristic can increase the interval between doses, provide greater comfort to the patient, and, consequently, greater adherence to treatment.

Studies show that magnetic nanoparticles of iron oxide (MPIO) can be used in biomedical applications due to their magnetic properties and biocompatibility. These nanoparticles are formed by iron oxides of maghemite (γ-Fe_2O_3) and magnetite (Fe_3O_4) (Khalafalla and Reimers 1980; Ramezani et al. 2022). They can be used in the form of colloidal dispersions stabilised by surfactants or polymers called magnetic fluids (MF) (Khalafalla and Reimers 1980; Yen et al. 2013; Ramezani et al. 2022). Studies address improvements in the efficiency and quality of magnetic resonance imaging diagnostics when MF is used as contrast (Kermanian et al. 2021). Among other advantages, the use of these nanosystems can enable the transport of drugs known for their side effects, due to the lack of specificity of their targets to the specific site of action (Bejjanki et al. 2021).

Still, further investigations are needed regarding the toxicity of iron oxide-based nanosystems. Bejjanki et al. (2021) show a nanosystem containing MPIO that uses folic acid for targeted transport of aggregated cisplatin to overcome cisplatin resistance in nasopharyngeal carcinoma. From another perspective, Zhu et al. (2021) present results demonstrating the aggravation of hepatic steatosis in liver inflammation in non-alcoholic fatty liver disease in mice and hepatocellular carcinoma (HepG2) cells, when in the presence of iron oxide.

In the present work, we evaluated the toxicity of rifampicin associated with iron oxide nanoparticles, by the *Artemia salina* lethality method, and we evaluated the antimicrobial activity of the nanocompounds against *Staphylococcus aureus*, with a disc diffusion test.

2. Material and Methods

Synthesis

The synthesis of iron oxide nanoparticles was performed with coprecipitation of 12 grams of $FeCl_2.4H_2O$ (J.T. Baker) and 24 grams of $FeCl_3.6H_2O$ (Synth) in an alkaline medium (25% ammonium hydroxide - Dinâmica Ltd.) under a mechanical stirring of 500 revolutions per minute (Khalafalla and Reimers 1980; Van Ewijk et al. 1999). The solid, black-colored sample resulting from this step was decanted under a neodymium magnet and the supernatant was removed. The pellet was functionalized by adding 2.0 g of lauric acid (AL) (Sigma-Aldrich) under mechanical stirring and heating (90 °C) for 20 minutes (Van Ewijk et al. 1999; Ferreira et al. 2015). The magnetic fluid resulting from this step was taken for oxidation of the particles via bubbled oxygen under heating (90 °C) for a period of 8 h (Kang et al. 1996). Then, the fluid was dialyzed by a semipermeable membrane and sterilised in an autoclave for 15 min at 121 °C. The sample resulting from this step had a pH of 7.4.

For the association process of the drug to the nanosystem, 22 mg of rifampicin were solubilized in 1 mL of previously sterilised dimethyl sulfoxide (DMSO), and then, the solution obtained was added to 10 mL of the nanosystem. This mixture remained under mechanical stirring for 48 h at room temperature. Afterward, it was submitted to magnetic separation with a neodymium magnet (400 Gauss) for 48 h under refrigeration (2 °C) and protected from light. The supernatant liquid resulting from this separation was used for quantification of free RIF, i.e., not incorporated into the nanosystem (Ferreira et al. 2015).

The RIF-nanosystem was collected in a dark flask and the volume was corrected with deionized and autoclaved water to 10 mL. The nanosystem was produced using the same procedure, placing a 10 mL aliquot of the magnetic fluid in 1 mL of pure DMSO. Aliquots of 100 µL from the nanosystem and the RIF-nanosystem sample were separated to quantify the concentration of iron ions.

Characterization

Atomic absorption spectroscopy (AAS) was used to determine the concentration of iron ions contained in the samples, nanosystem, and RIF-nanosystem, using *Perkin Elmer Analyst* 400 equipment.

The electronic absorption spectroscopy analysis in the ultraviolet-visible (UV-vis) region was used to determine the content of rifampicin not incorporated into the nanosystem. This analysis was performed in the Perkin Elmer UV-vis Spectrometer model Lambda (Rodríguez et al. 2014). The determination of the concentration of RIF adsorbed to the nanosystem was performed by an indirect method, i.e., by analysing the supernatant resulting from the magnetic separation step. To prepare an analytical standard curve for rifampicin, rifampicin standards were prepared, followed by their absorbance reading at 474 nm wavelength. The results are in agreement with those described in the Brazilian Pharmacopoeia for rifampicin (ANVISA 2019).

Fourier Transform (FTIR) vibrational absorption spectroscopy was used to identify the nature of the organic and inorganic materials contained in the studied samples. Alterations in the characteristic pattern of absorption bands clearly indicate a change in the material composition. The samples were previously lyophilized (L101 Liotop) to make KBr pellets, and in a Perkin Elmer Spectrum 400 spectrophotometer, with a spectral region between 4000 and 400 cm^{-1}.

X-ray diffractograms were obtained in a Shimadzu, model XRD 6000. The analyses were performed in the range of $10° ≤ 2θ ≤ 80°$, with a Cu-Kα radiation source (λ = 1.54056 Å), under a current of 30 mA, and a voltage of 40 kV, and at a scan rate of 2°/minute. The Zetasizer Nano ZS (Malvern Instruments) was used to characterise the hydrodynamic diameter of the particles, the zeta potential value (ζ), and the dispersion index (DI).

Biological tests

Toxicity assay with Artemia salina

Eighty milligrams of brine shrimp (*Artemia salina*) cysts were incubated for 36 h under natural lighting, room temperature, and constant aeration for the hatching of the larvae (nauplii) in synthetic seawater culture medium prepared by dissolving 40 $g.L^{-1}$ of sea salt, supplemented with yeast extract (6 $mg.L^{-1}$), sterilised in an autoclave and the pH adjusted to 8.5 with a 0.1 $mol.L^{-1}$ with Na_2CO_3 solution. After hatching the cysts, the larvae were distributed in wells of polystyrene plate, standardising 10 ± 1 individuals in each well (Ates et al. 2015; Machado et al. 2021). Then, 100 µL of each previously prepared dilution of the study compounds was added to these wells.

The lethality assay was used to determine the medium lethal concentration of the compounds for 50% of the population of *Artemia salina* (LC_{50}) (Machado et al. 2021). The assays were performed in 96-well polystyrene microplates with the concentrations of 800, 400, 200, 100, 50 $µg.mL^{-1}$ for free RIF, of 3000, 1500, 750, 124, 62.5 $µg.mL^{-1}$ of 550, 275, 135.5 and 68.76 $µg.mL^{-1}$ RIF-nanosystem. In addition to these, residual solvent control tests were performed with 5% DMSO, viability control with synthetic seawater, and technique control with potassium dichromate ($K_2Cr_2O_7$) at concentrations of 100, 50, 25, and 12.25 µg mL^{-1}.

After 24 h of exposure to the compounds, counts of live, dead, or immobile brine shrimp were performed in triplicate with three independent experiments. The results allowed the calculation of LC_{50} by the probit program StatplusPro V5 2015 professional (AnalystSoft) (Arulvasu et al. 2014; Machado et al. 2021).

Nguta et al. (2011) established that compounds with LC_{50} less than 100 $µg.mL^{-1}$ are classified as highly toxic compounds to artemia, those with LC_{50} between 100 $µg.mL^{-1}$ and 500 $µg.mL^{-1}$ with moderate

toxicity, those with LC_{50} between 500 µg.mL^{-1} and 1000 µg. mL^{-1} with low toxicity and those with LC_{50} greater than 1000 µg.mL^{-1} are classified as non-toxic.

Microscopic analysis

The brine shrimp were observed with a Leica DMRB microscope (Leica, Switzerland). Images were obtained using a Leica DFC420C CCD camera and Leica software (Leica Application Suite LAS EZ) and imagens of *A. salina* were taken at 100x magnification. The resulting images were stored and viewed in the Leica software program using the TIFF image format with a resolution of 1600 x 1200.

Disc Diffusion Test

The disk diffusion test was used to evaluate and compare the inhibitory activity of free RIF, nanosystem, and RIF-nanosystem. The assay followed the Clinical and Laboratory Standard Institute (CLSI 2011) recommendations for antimicrobial susceptibility testing of bacteria growing in aerobiosis (M7 2018) and the *Staphylococcus aureus* ATCC 25923 was tested.

Succinctly, bacterial suspensions were adjusted to 1.5 x 10^8 CFU.mL^{-1} with a 0.5 McFarland scale, and the inocula were plated on Mueller Hinton agar. Subsequently, filter paper discs previously impregnated with free rifampicin 5 µg.mL^{-1} and 500 µg.mL^{-1}, nanosystem 6000 µg.mL^{-1}, and iron and rifampicin 5 µg.mL^{-1} and 500 µg.mL^{-1} were placed on the surface of the inoculated medium. In addition to these compounds, gentamicin discs were used as a control technique. The plates were incubated at 35 °C for 24 h. The diameters of the inhibition zones were measured in millimetres. All experiments were performed in independent triplicates (Rodríguez et al. 2014).

3. Results

Characterization

Figure 1 presents the results obtained using vibrational absorption spectroscopy in the infrared region. The technique was used to obtain information regarding the functional groups and bonds present in the compounds (Casillas et al. 2012). In Figure 1a it is possible to observe a band at 587 cm^{-1}, which can be attributed to the Fe-O stretching vibration at tetrahedral and octahedral Fe-O-Fe sites in the maghemite (γ-Fe$_2$O$_3$) phase (Ishii et al. 1972; Nasrazadani and Raman 1993; Namduri and Nasrazadani 2008; Khan et al. 2022). And a band at 634 cm^{-1}, which can be attributed to Fe-O bond deformation at octahedral sites in the maghemite phase (Ishii et al. 1972; Nasrazadani and Raman 1993; Namduri and Nasrazadani 2008; Casillas et al. 2012). It is also observed in Figure 1b at the 1710 cm^{-1} band that corresponds to the symmetric and asymmetric C=O stretching of the COO$^-$ bond of the protonated carboxylic acid used to perform the functionalization of the sample (Arulvasu et al. 2014).

In Figure 1b, obtained for the RIF-nanosystem sample, it can be seen that the bands at 635 and 588 cm^{-1}, attributed to Fe-O bond deformation and Fe-O stretching at tetrahedral and octahedral Fe-O-Fe sites of γ-Fe$_2$O$_3$, did not undergo displacement when RIF is associated with the nanosystem. It can be further noted in Figure 1b that some characteristic bands of the free RIF, Figure 1c, did not undergo significant displacements, such as the bands 1643 cm^{-1} and 1457 cm^{-1}. These rifampicin bands can be attributed to asymmetric and symmetric stretching vibrations of carboxylate COO- groups, confirming the presence of rifampicin in the proposed nanosystem (Arulvasu et al. 2014; Parumasivam et al. 2016).

The presence of the bands at 1726 cm^{-1} and 1645 cm^{-1} in Figure 1c suggests that the crystalline structural form of rifampicin used in the experiments is not the polymorphic form II of RIF, due to the absence of the double signal around 1740 - 1710 cm^{-1}, attributed to the C=O bond of the acetyl group (Ibiapino et al. 2014). The double signal is also not observed for the RIF-nanosystem sample. It is thus expected that polymorphic I and/or amorphous forms may be present in the RIF-nanosystem sample, known to be thermodynamically more stable (Pelizza et al. 1977).
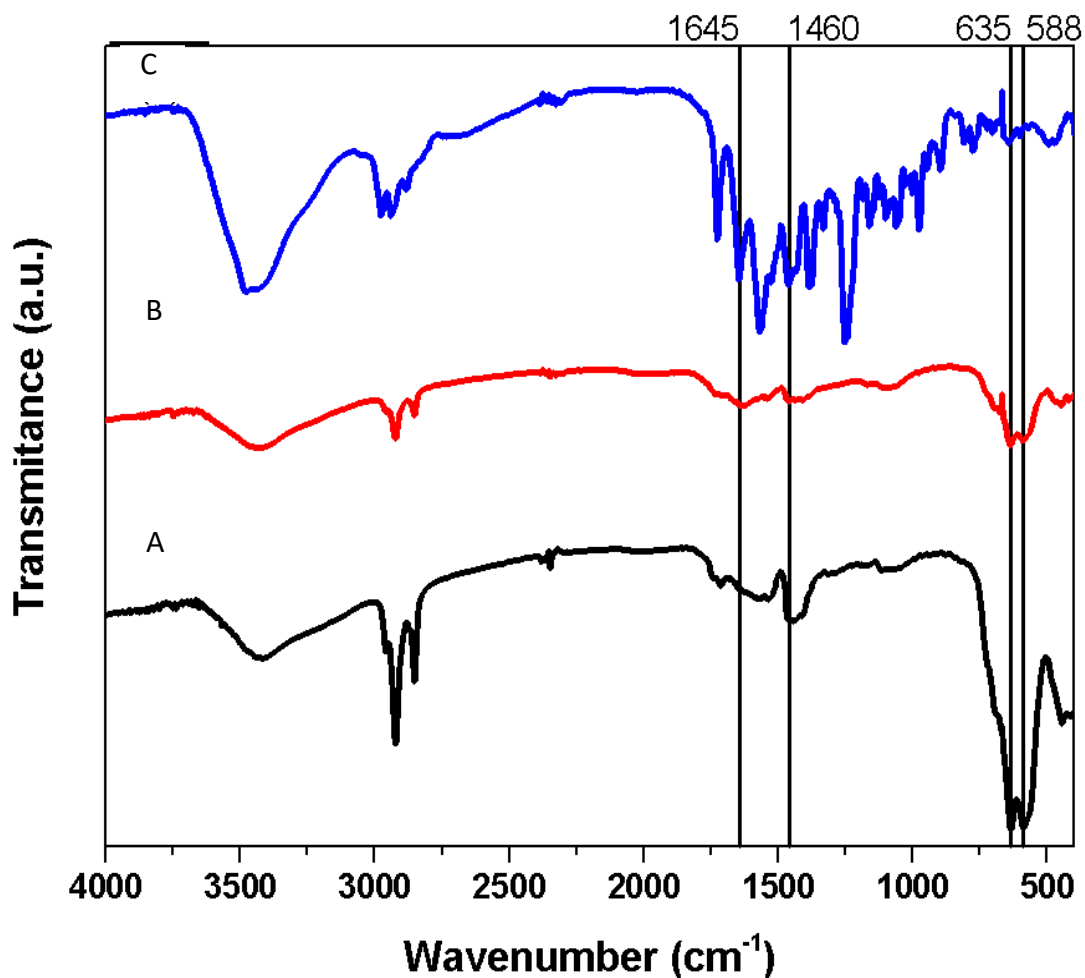
Figure 1. FTIR results for: A - nanosystem, B - RIF-nanosystem and C - free RIF.

The X-ray diffraction (XRD) technique was used to characterise the crystallographic phase of the iron oxide nanoparticles. It is possible to observe in Figure 2 the diffractogram of the nanosystem sample. The diffractogram shows peaks at 30.12°; 35.80°; 43.46°; 57.34°; 63.08° and 74.60° reflections that can be indexed to the planes of the crystal lattice determined by (220), (311), (400), (422), (511), and (440); which correspond to the intensity of the diffracted waves as a function of angle 2θ for an inverse spinel-type structure, characteristic of the iron oxides phase: magnetite Fe_3O_4 (ICCD 019-0629) and/or maghemite γ-Fe_2O_3 (ICCD 39-1346). The majority phase present in the nanosystem is expected to be maghemite since the samples underwent an eight-hour oxidation process.

The Debye-Scherrer equation (CULLITY and STOCK 2001) was used to estimate the average diameter of the particles present in the nanosystem samples.

$$D = \frac{0,9\lambda}{\beta \cos\theta}$$

Where *D* is the crystallite diameter; 0.9 is the correction factor; λ is the X-ray wavelength; θ is the diffraction angle of the most intense peak and *β* is the half-height width of the most intense diffraction peak.

In this study, the value of *β* used was obtained for the most intense peak (311). The calculated value for the average diameter of the particles comprising the nanosystem was 8.37 nm.
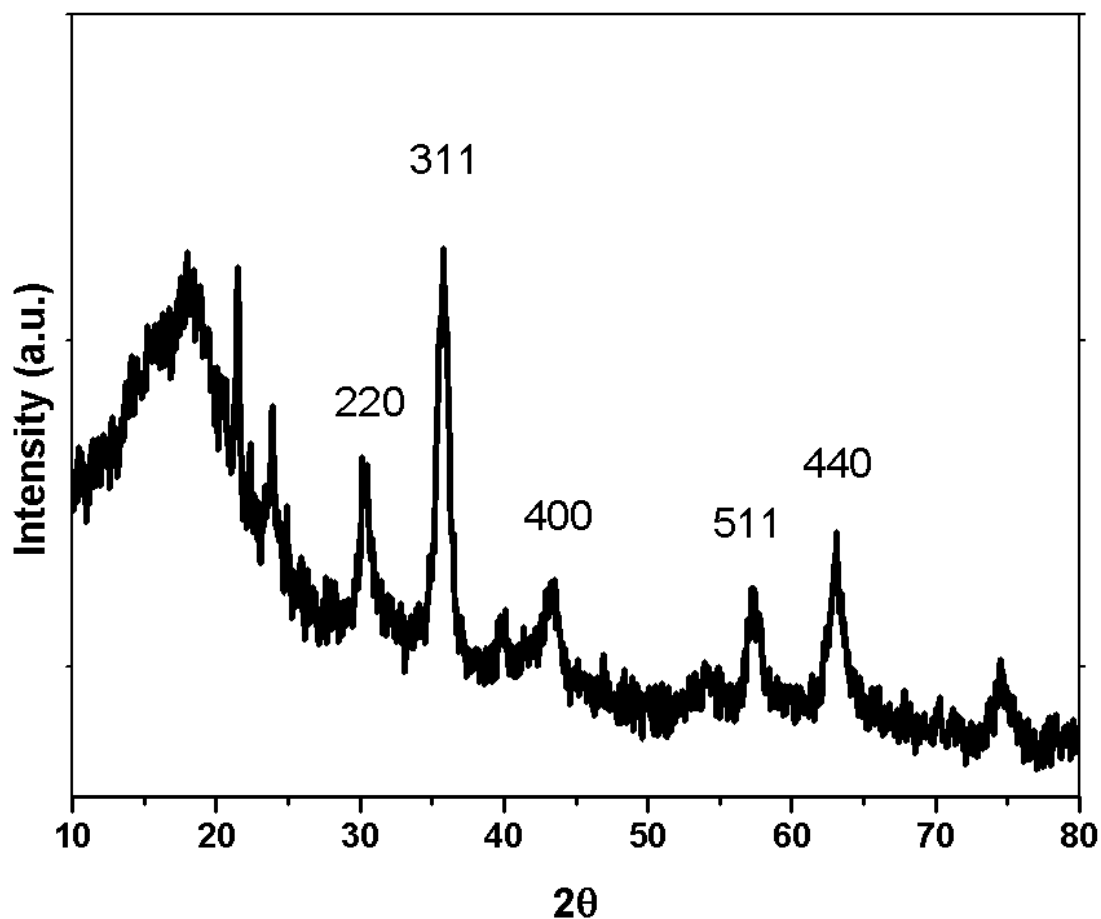
Figure 2. X-ray diffractometry of the nanosystem.

Through the dynamic light scattering technique, it was possible to characterise the nanosystem and RIF-nanosystem samples regarding hydrodynamic size, zeta potential, and dispersion index (DI). The result found for the hydrodynamic diameter of the nanosystem was 56.89 mm and a DI of 0.212. While for RIF-nanosystem the hydrodynamic diameter was 406 mm and the was DI 0.615. It is observed that the RIF-nanosystem showed a hydrodynamic size larger than the nanosystem. It is suggested that it is due to the adsorption of RIF to the nanosystem (Santos et al. 2011) and that a higher DI value for RIF-nanosystem is a consequence of the formation of possible aggregate during the adsorptive process. A schematic proposal for RIF-nanosystem can be consulted in previous works of the research group (Santos et al. 2011).

The colloidal stability of the samples was evaluated based on the determination of the zeta potential (ζ). It was observed that the value of ζ for the RIF-nanosystem was -22.0 mV while for the nanosystem was -15.2 mV. These values of ζ suggest the occurrence of the repulsive force between the particles, favouring their stability (Riddick 1968; Arulvasu et al. 2014). The addition of RIF to the nanosystem reduced the ζ values suggesting that the colloidal dispersion disfavors the colloidal stability of the nanosystem.

The iron ion concentration obtained by AAS was 6 mg.mL^{-1} for both samples, this value does not differ from the other results obtained in other studies (Santos et al. 2011). The concentration of rifampicin in the RIF-nanosystem was determined by UV-vis was 1.1 mg.mL^{-1}.

Lethality assay to *Artemia salina*

Rifampicin showed LC$_{50}$ to artemia at 312.94 µg.mL^{-1}, and 535.38 µg.mL^{-1} to rifampicin - associated with the nanosystem, with classification to the toxicity or moderate and low, respectively. The nanosystem was considered non-toxic and no artemia mortality was observed in wells with 5% DMSO and viability controls with synthetic seawater. Potassium dichromate showed LC$_{50}$ of 45 µg.mL^{-1}. The results of the toxicity assay of the compounds to *Artemia salina* are shown in Table 1.

Table 1. Medium lethal concentration of the compounds to *Artemia salina*.

Compounds	LC$_{50}$ (µg.mL^{-1})	Classification Toxicity
Rifampicin	312.94	Moderate toxicity
Rifampicin - nanosystem	535.38	Low toxicity
Nanosystem	≥ 3,000	Non-toxic

Antimicrobial activity of the compounds

In Table 2 is possible to observe that the nanosystem did not show a halo of inhibition on the growth of *Staphylococcus aureus* and that the RIF-nanosystem at the concentration of 5 µg.mL^{-1} showed a halo 11.76% smaller than free RIF 5 µg.mL^{-1}. The same phenomenon was observed for the concentration of 500 µg.mL^{-1}, with a decrease of 8.82% of the halo compared to free RIF.

Table 2. Diameters of inhibition halos of *Staphylococcus aureus* ATCC 25923 by the tested compounds.

Compounds	Concentration (µg.mL^{-1})	Halo (mm)
Rifampicin	500	34,33±0,58
Rifampicin	5	16,67±0,58
RIF-nanosystem	500	30,67±1,15
RIF-nanosystem	5	14,67±2,08
Nanosystem	6,000	0

Microscopic analysis of *Artemia salina*

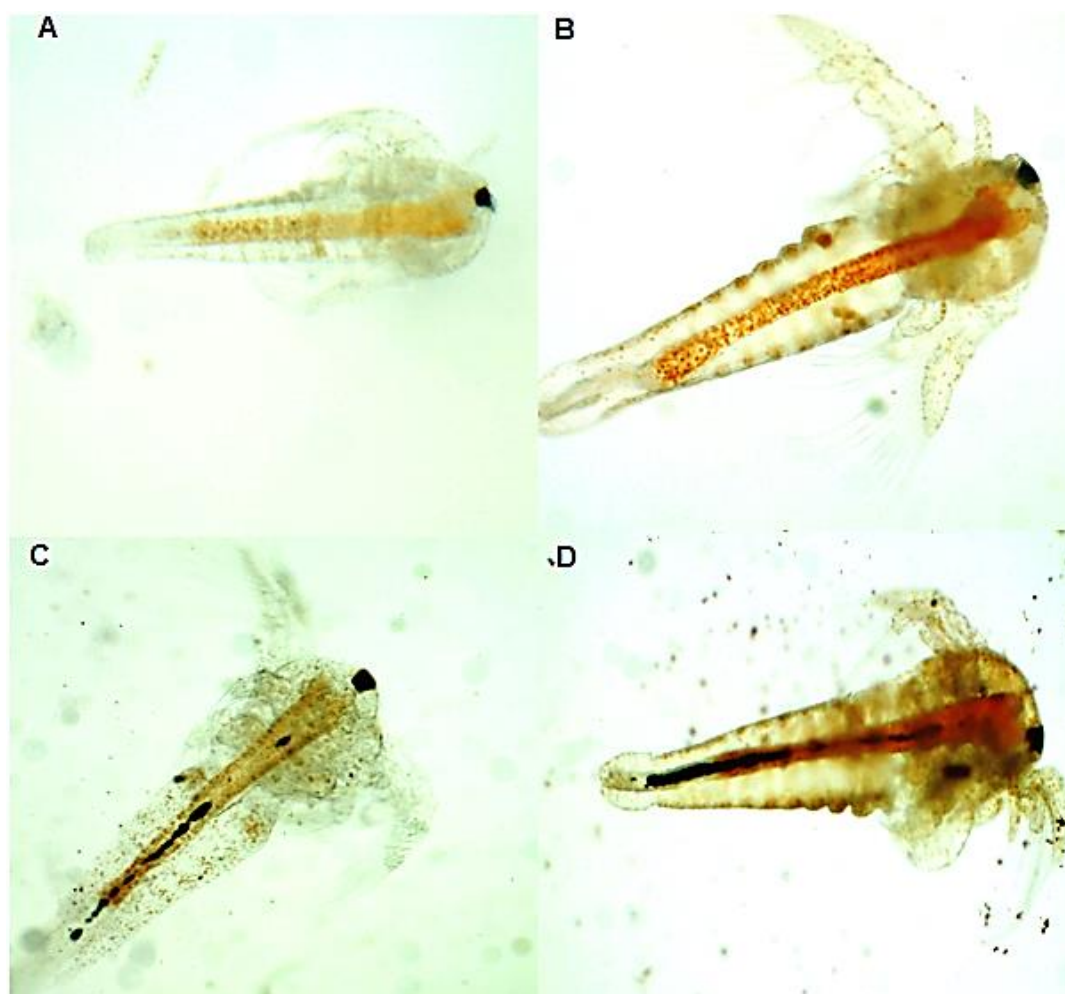The microscopy image in Figure 3 shows the artemia after exposure to the evaluated compounds.

Figure 3. Microscopy image (100x magnification) of *Artemia salina* after exposure to the compounds: A - unexposed control, B - Rifampicin, C - Nanosystem and D - Rifampicin - Nanosystem.

4. Discussion

The characterization techniques confirm the presence of iron oxide in the maghemite phase. The techniques used show that it was possible to functionalize the synthesised iron oxide with lauric acid. Furthermore, it was confirmed that rifampicin is associated with the nanosystem and that this association indicates that the nanosystem can transport the drug. The considerable increases in the hydrodynamic diameter and the dispersivity index for RIF-nanosystem compared to the nanosystem without the drug, suggest that the drug associated with the nanosystem can promote particle aggregation. The addition of RIF to the nanosystem reduced the ζ values suggesting that the colloidal dispersion does not favour the colloidal stability of the nanosystem (Santos et al. 2011; Arulvasu et al. 2014).

The nanosystem fluid was non-toxic and showed LC_{50} greater than 3,000 µg.mL^{-1} as observed by Gambardella et al. (2014) and Rajabi et al. (2015). In the present study, we observed that there was a 41.54% reduction in the toxicity of rifampicin when associated with the nanosystem to the *A. salina*. Xiong et al. (2015) found that nanoparticles could inactivate free radicals and decrease injury to lipid membranes in guinea pigs. One of the problems concerning rifampicin is nephrotoxicity (Min et al. 2013) and hepatological (Legout et al. 2014) side effects.

Rajabi et al. (2015) evidenced that the results obtained with the toxicity assay in *Artemia salina* showed no statistical difference ($p > 0.05$) compared to those obtained with the MTT assay. These findings suggest that the *Artemia salina* assay can accelerate toxicity studies, decrease costs, and therefore be considered a viable alternative to the in vitro cell culture assay (Ntungwe et al. 2020).

Artemia salina is considered a non-selective filterer and can easily ingest particles up to 50 µm in diameter (Ates et al. 2013; Rodd et al. 2014). However, it was observed that the presence of the compounds inside the microcrustaceans did not induce mortality after 24 h of exposure (Cornejo-Garrido et al. 2011). Furthermore, artemias treated with nanosystem alone remained alive after the 72 h incubation period, while artemias exposed to rifampicin, rifampicin - nanosystem, and the DMSO control did not survive after the same exposure period.

The toxicity of Fe_3O_4 nanoparticles was evaluated in ethological parameters of *A. salina* and was related to oxidative stress, as ROS species, malondialdehyde content, total antioxidant capacity and antioxidant activities increased significantly. In addition, mitochondrial malformation was observed after exposure to Fe_3O_4-NPs (Zhu et al. 2017).

Behaviour changes were visualised in the artemia exposed to the nanosystem and rifampicin-nanosystem, which were more agitated than those in the untreated control. These observations were also described by Gambardella et al. (2014) in the presence of Fe_3O_4 nanoparticles. These authors also demonstrated an increase in biochemical responses, catalase and cholinesterase activities that may be correlated with inflammation and that the stress recorded by the larvae was due to an increase in cholinesterase and not ROS.

In other studies, increases in cholinesterase and catalase were also identified in artemias. It is known that cholinesterase can function as a regulator of inflamed tissue (Falugi et al. 2012), suggesting that iron oxide nanoparticles have antioxidant mechanisms in preventing oxidative damage (Huang et al. 2013).

5. Conclusions

In the present study, a magnetic colloidal dispersion consisting of iron oxide nanoparticles stabilised with lauric acid and associated rifampicin was obtained and characterised by spectroscopic techniques, confirming the functionalization of lauric acid on the surface of the particles and the adsorption of rifampicin to the system. In addition, the analytical methods provided an estimate of the average diameter of the nanoparticles and determined the presence of maghemite in the nanosystem.

Regarding the biological activities evaluated, it was possible to observe that there was a reduction of rifampicin toxicity when associated with iron oxide nanoparticles, as detected by lethality assay with *Artemia salina* and that the in vitro antimicrobial activity of rifampicin, when associated with

nanoparticles, was slightly reduced when compared to free rifampicin against *Staphylococcus aureus* ATCC 25923.

Overall, the results demonstrated that the nanosystems showed no toxicity to *Artemia salina* and may have the potential for use as a platform for reducing the toxicity of associated drugs. Therefore, we suggest that additional studies should be conducted to corroborate the results found in this study.

References

ADAMS, R.A., et al. Rifamycin antibiotics and the mechanisms of their failure. *The Journal of Antibiotics*. 2021, **74**(11), 786-798. https://doi.org/10.1038/s41429-021-00462-x

ARULVASU, C., et al. Toxicity effect of silver nanoparticles in brine shrimp Artemia. *The Scientific World Journal*. 2014, **2014**, 256919. https://doi.org/10.1155/2014/256919

ATES, M., et al. Evaluation of Alpha and Gamma Aluminum Oxide Nanoparticle Accumulation, Toxicity and Depuration in *Artemia salina* Larvae Mehmet. *Environmental Toxicology*. 2015, **141**(4), 520–529. https://doi.org/10.1002/tox.21917

ATES, M., et al. Comparative evaluation of impact of Zn and ZnO nanoparticles on brine shrimp (*Artemia salina*) larvae: effects of particle size and solubility on toxicity. *Environmental Science: Processes Impacts*. 2013, **15**(1), 225–233. https://doi.org/10.1039/C2EM30540B

ANVISA. BRAZILIAN PHARMACOPOEIA - Agência Nacional de Vigilância Sanitária –, 6th edition. *Farmacopeia Brasileira*. Brasília-DF, Editora Fiocruz, 2019. Approved by RDC n. 298 of August 2019. https://www.gov.br/anvisa/pt-br/assuntos/farmacopeia/farmacopeia-brasileira

BEJJANKI, N.K., et al. GSH triggered intracellular aggregated-cisplatin-loaded iron oxide nanoparticles for overcoming cisplatin resistance in nasopharyngeal carcinoma. *Journal of Biomaterials Applications*. SAGE Publications Ltd STM. 2021, **36**(1), 45–54. https://doi.org/10.1177/0885328220982151

CASILLAS, P.E.G., et al. Infrared Spectroscopy of Functionalized Magnetic Nanoparticles. *In*: Theophanides, T. *Infrared Spectroscopy - Materials Science*, *Engineering and Technology*. London: IntechOpen. 2012, 405–420.

CLSI. Methods for Dilution Antimicrobial Susceptibility Tests for Bacteria That Grow Aerobically; Approved Standard— Eleventh Edition. CLSI document M07. Wayne, PA: *Clinical and Laboratory Standards Institute*; 2018.

CORNEJO-GARRIDO, H., et al. Oxidative stress, cytotoxicity, and cell mortality induced by nano-sized lead in aqueous suspensions. *Chemosphere*. 2011, **84**(10), 1329–1335. https://doi.org/10.1016/j.chemosphere.2011.05.018

CULLITY, B.D. and STOCK, S.R. *Elements of X-ray Diffraction*, Third Edition. 3rd ed. New York: Prentice-Hall; 2001.

FALUGI, C., et al. Toxicity of metal oxide nanoparticles in immune cells of the sea urchin. Marine Environmental Research. Elsevier. 2012, **76**, 114–121. https://doi.org/10.1016/J.MARENVRES.2011.10.003

FERREIRA, Q.S., et al. Rifampicin adsorbed onto magnetite nanoparticle: SERS study and insight on the molecular arrangement and light effect. *Journal of Raman Spectroscopy*. John Wiley & Sons, Ltd. 2015, **46**(9), 765–771. https://doi.org/10.1002/jrs.4718

GAMBARDELLA, C., et al. Effects of selected metal oxide nanoparticles on *Artemia salina* larvae: evaluation of mortality and behavioral and biochemical responses. Environmental Monitoring and Assessment. *Environmental Monitoring and Assessment*. 2014, **186**(7), 4249–4259. http://doi.org/10.1007/s10661-014-3695-8

GOLDSTEIN, B.P. Resistance to rifampicin: a review. *The Journal of antibiotics*. 2014, **67**(9), 625-630. https://doi.org/10.1038/ja.2014.107

HUANG, G., et al. Superparamagnetic Iron Oxide Nanoparticles: Amplifying ROS Stress to Improve Anticancer Drug Efficacy. *Theranostics*. Ivyspring International Publisher. 2013, **3**(2), 116. https://doi.org/10.7150/THNO.5411

IBIAPINO, A.L., et al. Structural characterization of form I of anhydrous rifampicin. *CrystEngComm*. The Royal Society of Chemistry. 2014, **16**(36), 8555–8562. https://doi.org/10.1039/C4CE01157K

ISHII, M., et al. Infrared absorption spectra and cation distributions in (Mn, Fe)$_3$O$_4$. *Solid State Communications*. Pergamon, 1972, **11**(1), 209–212. https://doi.org/10.1016/0038-1098(72)91162-3

KANG, Y.S., et al. Synthesis and characterization of nanometer-size Fe$_3$O$_4$ and γ-Fe$_2$O$_3$ particles. *Chemistry of Materials*. American Chemical Society. 1996, **8**(9), 2209–2211. https://doi.org/10.1021/cm960157j

KHAN, M.I., et al. Recent Progress in Nanostructured Smart Drug Delivery Systems for Cancer Therapy: A Review. *ACS Applied Biomaterials*. 2022, **2022**. https://doi.org/10.1021/acsabm.2c00002

KHALAFALLA, S. and REIMERS, G. Preparation of dilution-stable aqueous magnetic fluids. Magnetics, IEEE Transactions on. 1980, **2**, 178–183. https://doi.org/10.1109/TMAG.1980.1060578

KERMANIAN, M., et al. Inulin-Coated Iron Oxide Nanoparticles: A Theranostic Platform for Contrast-Enhanced MR Imaging of Acute Hepatic Failure. *ACS Biomaterials Science & Engineering*. 2021, **7**(6), 2701–2715. https://doi.org/10.1021/acsbiomaterials.0c01792

LAURENT, S., et al. Magnetic iron oxide nanoparticles: Synthesis, stabilization, vectorization, physicochemical characterizations and biological applications. Chemical Reviews. 2008, **108**(6), 2064–2110. https://doi.org/10.1021/cr068445e

LEGOUT, L., et al. Factors predictive of treatment failure in staphylococcal prosthetic vascular graft infections: a prospective observational cohort study: impact of rifampin. *BMC infectious diseases*. 2014, **14**(1), 1-9. https://doi.org/10.1186/1471-2334-14-228

MACHADO, A.J.T., et al. Single and combined toxicity of amino-functionalized polystyrene nanoparticles with potassium dichromate and copper sulfate on brine shrimp *Artemia franciscana* larvae. *Environmental Science and Pollution Research*. 2021, **28**(33), 45317–45334. https://doi.org/10.1007/s11356-021-13907-5

MOTTA, J.C., et al. Acute tubulointerstitial nephritis due to the use of rifampicin. Case report. 2020, **6**(1), 44-51. https://doi.org/10.15446/cr.v6n1.80443

NAMDURI, H. and NASRAZADANI, S. Quantitative analysis of iron oxides using Fourier transform infrared spectrophotometry. *Pergamon*. 2008, **50**(9), 2493–2497. https://doi.org/10.1016/J.CORSCI.2008.06.034

NASRAZADANI, S. and RAMAN, A. The application of infrared spectroscopy to the study of rust system-II. Study of cation deficiency in magnetite (Fe$_3$O$_4$ produced during its transformation to Maghemite (γ-Fe$_2$O$_3$) and hematite (α-Fe$_2$O$_3$). *Corrosion Science*. 1993, **34**(8), 1355–1365. https://doi.org/10.1016/0010-938X(93)90092-U

MIN, H.K., et al. Rifampin-associated tubulointerstitial nephritis and Fanconi syndrome presenting as hypokalemic paralysis. *BMC Nephrology*. 2013, **14**(1), 13. https://doi.org/10.1186/1471-2369-14-13

NGUTA, J.M., et al. Biological screening of Kenya medicinal plants using *Artemia salina* (ARTEMIIDAE). *Pharmacologyonline*. 2011, **2**, 458–78. http://erepository.uonbi.ac.ke:8080/xmlui/handle/123456789/9787

NTUNGWE, N.E., et al. Artemia species: An important tool to screen general toxicity samples. *Current Pharmaceutical Design*. 2020, **26**(24), 2892-2908. https://doi.org/10.2174/1381612826666200406083035

PARUMASIVAM, T., et al. Rifapentine-loaded PLGA microparticles for tuberculosis inhaled therapy: preparation and in vitro aerosol characterization. *European Journal of Pharmaceutical Sciences*. 2016, **88**, 1-11. https://doi.org/10.1016/j.ejps.2016.03.024

PELIZZA, G., et al. Polymorphism of rifampicin. *Il Farmaco, Edizione Scientifica*. PMID: 891903 1977, **32**(7), 471–481.

PERUMAL, R., et al. A systematic review and meta-analysis of first-line tuberculosis drug concentrations and treatment outcomes. *The International Journal of Tuberculosis and Lung Disease*. 2020, **24**(1), 48-64. https://doi.org/10.5588/ijtld.19.0025

RAJABI, S., et al. *Artemia salina* as a model organism in toxicity assessment of nanoparticles. DARU *Journal of Pharmaceutical Sciences*. 2015, **23**(1), 20. https://doi.org/10.1186/s40199-015-0105-x

RAMEZANI, F.M., et al. Folic Acid-Adorned Curcumin-Loaded Iron Oxide Nanoparticles for Cervical Cancer. *ACS Applied Biomaterials*. 2022, **5**(3), 1305–1318. https://doi.org/10.1021/acsabm.1c01311

RIDDICK, T.M. *Control of colloid stability through zeta potential*. 1st ed. Livingston Pub Wynnewood: Zeta-Meter - Livingston Pub.; 1968.

RODRÍGUEZ, A., et al. Characterization of antibacterial and hemolytic activity of synthetic pandinin 2 variants and their inhibition against *Mycobacterium tuberculosis*. *PLOS ONE*. Public Library of Science. 2014, **9**(7). https://doi.org/10.1371/JOURNAL.PONE.0101742

RODD, A.L., et al. Effects of surface-engineered nanoparticle-based dispersants for marine oil spills on the model organism *Artemia franciscana*. *Environmental science & technology*. 2014, **48**(11), 6419–6427. https://doi.org/10.1021/es500892m

RUCKH, T.T., et al. Antimicrobial effects of nanofiber poly(caprolactone) tissue scaffolds releasing rifampicin. *Journal of Materials Science: Materials in Medicine*. 2012, **23**(6), 1411–20. https://doi.org/10.1007/s10856-012-4609-3

SANTOS, C.M.B., et al. SERRS study of molecular arrangement of amphotericin b adsorbed onto iron oxide nanoparticles precoated with a bilayer of lauric acid. *Journal of Physical Chemistry* C. 2011, **115**(42), 20442–20228. https://doi.org/10.1021/jp206434j

VAN EWIJK, G.A., VROEGE, G.J. and PHILIPSE, A.P. Convenient preparation methods for magnetic colloids. *Journal of Magnetism and Magnetic Materials*. Elsevier, 1999, **201**(1–3), 31–3. https://doi.org/10.1016/S0304-8853(99)00080-3

WOŹNIAK-BUDYCH, M.J., et al. Green synthesis of rifampicin-loaded copper nanoparticles with enhanced antimicrobial activity. *Journal of Materials Science: Materials in Medicine*. 2017, **28**(3), 1-16. https://doi.org/10.1007/s10856-017-5857-z

XIONG, F., et al. Cardioprotective activity of iron oxide nanoparticles. *Scientific Reports.* 2015, **5**(1), 1-8. https://doi.org/10.1038/srep08579

YEN, S.K., PADMANABHAN, P. and SELVAN, S.T. Multifunctional Iron Oxide Nanoparticles for Diagnostics, Therapy and Macromolecule Delivery. *Theranostics*. 2013, **3**(12), 986–1003. https://dx.doi.org/10.7150%2Fthno.4827

ZHU, S., et al. Developmental toxicity of Fe_3O_4 nanoparticles on cysts and three larval stages of *Artemia salina. Environmental Pollution*. 2017, **230**, 683-691. https://doi.org/10.1016/j.envpol.2017.06.065

ZHU, M., et al. Iron oxide nanoparticles aggravate hepatic steatosis and liver injury in nonalcoholic fatty liver disease through BMP-SMAD-mediated hepatic iron overload. *Nanotoxicology.* 2021, **15**(6), 761–778. https://doi.org/10.1080/17435390.2021.1919329